Predicting Nanocrystal Shape through Consideration of Surface-Ligand Interactions

Clive R. Bealing,[†,*] William J. Baumgardner,[‡] Joshua J. Choi,[§] Tobias Hanrath,[⊥] and Richard G. Hennig[†]

[†]Department of Materials Science and Engineering, [‡]Department of Chemistry and Chemical Biology, [§]School of Applied and Engineering Physics, and [⊥]School of Chemical and Biomolecular Engineering, Cornell University, Ithaca, New York 14853, United States

ABSTRACT

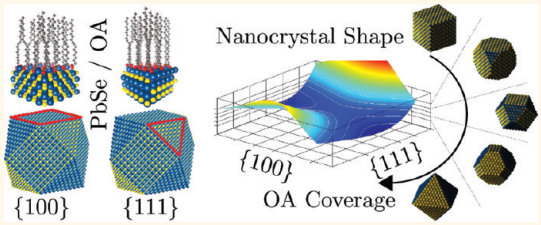

Density functional calculations for the binding energy of oleic acid-based ligands on Pb-rich {100} and {111} facets of PbSe nanocrystals determine the surface energies as a function of ligand coverage. Oleic acid is expected to bind to the nanocrystal surface in the form of lead oleate. The Wulff construction predicts the thermodynamic equilibrium shape of the PbSe nanocrystals. The equilibrium shape is a function of the ligand surface coverage, which can be controlled by changing the concentration of oleic acid during synthesis. The different binding energy of the ligand on the {100} and {111} facets results in different equilibrium ligand coverages on the facets, and a transition in the equilibrium shape from octahedral to cubic is predicted when increasing the ligand concentration during synthesis.

KEYWORDS: nanocrystal shape · PbSe · oleic acid · density functional theory · Wulff construction

The electronic, optical, and catalytic properties of nanocrystals (NCs) are highly tunable through adjustment of the NC size, shape, and composition[1−3] and are heavily influenced by the capping layer of organic surfactant ligands. NCs with a wide variety of shapes have been synthesized;[4−9] shape has normally been tuned either by kinetically controlling the growth of particular crystal facets[5,7,8,10] or through an oriented attachment mechanism.[6,9,11] The capping ligands play an important role in determining NC shape, which still requires clarification.

A better understanding of NC surface chemistry is increasingly recognized as an important problem,[12−16] being critical for a broad range of issues, including charge transport,[17−21] functionalization (*e.g.*, for biological systems),[22−26] optical properties (*e.g.*, quantum yield),[27−29] and the assembly of NCs into ordered structures.[30−32] Analysis of the effect of the ligands on the NC is perfectly suited to atomistic computational methods, whereas it is difficult to accomplish even with advanced synthesis tools, which are generally designed for the characterization of well-defined planar interfaces.

NC shape is controlled by the thermodynamics and growth kinetics of the dynamic system composed of the inorganic core, the ligands, and the solution containing chemical precursors and ligand species.[10,13,33] Shape control of NCs during growth is commonly understood as a kinetically controlled process: at high growth rates, ligands that selectively adhere to particular NC facets decrease their energy and slow their growth.[10] High-energy facets grow more quickly than low-energy facets in this kinetic regime and vanish as the NC grows, leading to NCs that are terminated by slow-growing low-energy facets.

In thermodynamic equilibrium, the shape of a NC is obtained by minimizing the surface energy for a given volume according to the Wulff construction.[33−35] Considering the NC surface−ligand problem, the surface energy of the various NC facets depends on both the ligand adsorption energy and coverage as well as the surface energy associated with the unpassivated surface. The adsorption energy is dominated by the chemistry of the ligand and NC. The equilibrium coverage is determined by the adsorption energy and external conditions such as temperature and ligand concentration. Hence, controlling the ligand coverage of the different facets through ligand concentration and temperature presents a potential route to control the equilibrium NC shape and could eliminate the need for a

* Address correspondence to crb242@cornell.edu.

Received for review October 15, 2011 and accepted February 13, 2012.

Published online February 13, 2012
10.1021/nn3000466

ligand that selectively adheres to a particular facet. This is important since the range of ligands known to exhibit such facet specificity is limited, and their identification is not straightforward.[36]

A NC system that has generated particular interest is that of the lead salts, for which the large exciton Bohr radius[37] and tunable interparticle spacing[18] and morphology[32] mean that assemblies of Pb-salt NCs are good candidates for photovoltaic and optoelectronic applications.[38−45]

The self-assembly of NCs into ordered macroscopic arrays or superlattices presents a route to novel functional materials. The self-assembly is controlled by the ligand-mediated interaction between neighboring NCs. Different ligand coverages on different NC facets can lead to anisotropic interactions between NCs by changing their effective shape. PbS NCs have been observed to pack into superlattices of different symmetry, depending on their degree of aging in solution, due to selective detachment of OA ligands from the {100} facets of the rocksalt (RS) core.[32] The need for rational control of NC shape and facet-specific ligand coverage calls for a broad theoretical understanding and computational study of the complex NC−ligand system.

Here we analyze how the NC surface coverage relates to the equilibrium shape of the inorganic core and the effective shape of the NC−ligand complex. Density functional calculations for oleic acid (OA), a common surfactant, on PbSe surfaces show that the ligand adsorption energy strongly depends on ligand coverage and facet type.

OA binds to the NC at surface Pb ions,[13] although the molecular form in which the ligand binds at the surface is not obvious, being either the neutral form or the deprotonated form, as oleate (OA^-) anions ($C_{17}H_{33}COO^-$). Calculations using density functional theory (DFT) for PbSe surfaces show that carboxylate-based ligands bind far more strongly to surface Pb ions than their carboxylic acid-based analogues and bind significantly more strongly to the PbSe {111} surface than to the {100} surface, reducing the gap between the bare surface energies.[46] This result is consistent with the fact that Pb-salt NCs, grown in the presence of OA, often exhibit {111} and {100} facets that are comparable in size.[47,48] It also opens up the possibility that the equilibrium NC core shape can be controlled by changing the concentration of OA during synthesis. The difference in binding energies of the ligand on the {100} and {111} facets results in different equilibrium ligand coverages and a transition in the equilibrium shape of the NC core from octahedral to cubic with increased ligand concentration during synthesis. The relative coverage of the different NC facets is predicted to be highly sensitive to the ligand concentration, suggesting that it is also possible to alter the core−ligand effective shape and, hence, the interactions between neighboring NCs.

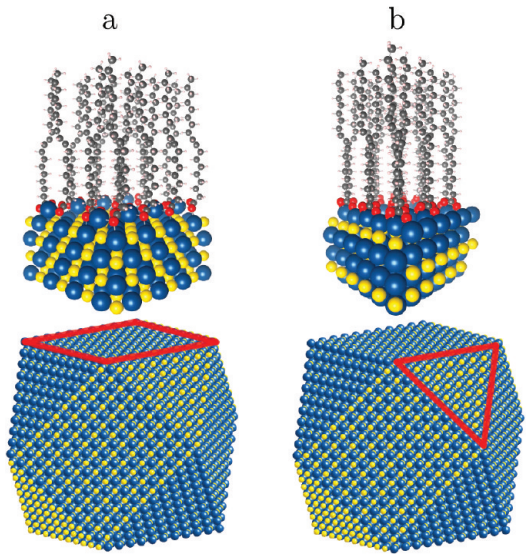

Figure 1. $Pb(OA^-)_2$ ligands attached to PbSe (a) {100} and (b) *R* {111} surfaces. Model NC cores are shown with a corresponding facet indicated in each case. Pb atoms are shown in blue, Se atoms in yellow, C in gray, O in red, and H in white.

Dispersed PbSe NCs exhibit only small net charges ranging from $-1e$ to $+2e$.[49] This near-zero charge on the NCs requires that the negative charge of the anionic ligands is compensated by surplus cations, most likely provided by an excess of Pb ions. Indeed, PbSe NC surfaces have been observed to be Pb-rich.[50−52] One excess surface Pb^{2+} cation for every two OA^- anions would yield NCs with zero net charge; a slight deviation from this proposed ionic environment on the NC surface would result in NCs with a small number of noncompensated charges, consistent with experiments in which OA^- anions have been observed to detach from the surface of PbSe NCs together with Pb cations, in the form of lead-oleate ($Pb(OA^-)_2$).[13] In light of these results, our study is concerned with OA^- and Pb^{2+} ions at PbSe surfaces, as opposed to OA or OA^- ligands interacting with stoichiometric PbSe surfaces.

RESULTS AND DISCUSSION

We build a thermodynamic model based on the Wulff construction and calculations of the ligands' adsorption energy. We argue that if the ligands occur as deprotonated OA^- anions on the Pb-rich NC surface,[13,46,49] they must be bound to excess Pb^{2+} cations, as illustrated by Figure 1. We predict that altering the ratio of Pb to OA during growth of Pb-salt NCs will enable the control of the relative coverage of the {100} and {111} facets such that the NC core shape may be tuned from a cube to a cuboctahedron to an octahedron, in agreement with an experimental study.[53] Isotherms reveal that the coverage of the {100} facets is predicted to be particularly sensitive

to the amount of surfactant present, suggesting that the effective shape of the NC core–ligand system can be altered by tuning the ligand density on these facets.

We determine the energy of the interaction of the ligands with the PbSe NC facets using DFT. Slab models of the PbSe {100} and {111} surfaces are used, each containing four Pb–Se layers, and are terminated by {100} and {111} surfaces, respectively. While {110} facets have sometimes been observed in Pb-salt NCs,[9,18,48] in this study the {110} facets are neglected. The lattice constant of bulk PbSe is calculated to be 6.204 Å. We use the bulk geometry to fix the position of the Pb and Se ions except for those in the topmost layer of the slab during relaxations, to reduce elastic interactions between the two slab surfaces. For the {111} surface, we consider the reconstructed Pb-terminated surface structure, here denoted *R* {111}.[48] This reconstruction significantly lowers the surface energy by moving half the Pb ions of the Pb-terminated {111} surface layer of the slab to the opposing Se-terminated surface, such that both terminating layers of the reconstructed slab are Pb-terminated, and each contains 50% of the Pb ions relative to the bulk layers. While the exact structure of the PbSe surface has yet to be determined experimentally, Rutherford-backscattering data suggest that the reconstruction employed here is similar to the real surface structure; epitaxially grown PbSe {111} layers were observed to be Pb-terminating, with the density of Pb in the terminating layer equal to 40% of a monolayer.[54] Our calculated surface energies for the uncapped PbSe {100} and *R* {111} surfaces are γ^0_{100} = 11.4 and γ^0_{111} = 20.4 meV/Å^2, similar to results by Fang *et al.*[48] of 11.4 and 20.5 meV/Å^2. We also considered the alternative "octupolar" reconstruction of the {111} surface,[55,56] which gave a comparable surface energy of 20.7 meV/Å^2.

In our study we consider both acetate (AA^-) and oleate (OA^-) ligands to determine the effect of the alkyl tail length on the adsorption energy. We treat an excess Pb^{2+} cation and two AA^- or OA^- anions together as the ligand group, resulting in lead acetate, $Pb(CH_3COO)_2$, and lead oleate, $Pb(CH_3(CH_2)_7CH{=}CH(CH_2)_7COO)_2$, ligands. Substituting the smaller AA^- for OA^- allows for efficient calculation of favorable ligand geometries and adsorption energies, by first relaxing the structures for AA^- and then substituting the long alkyl tail of OA^- for the methyl group. For a particular PbSe slab, the ligands were positioned above the surface, and the top Pb and Se layers and ligands were relaxed while keeping the remaining PbSe layers fixed.

The binding energies $E_{b,hkl}$ for the $Pb(AA^-)_2$ and $Pb(OA^-)_2$ ligands on the {*hkl*} surface of PbSe, neglecting solvent effects, are given as

$$E_{b,\,hkl} = (E_{\text{ligand}} + E_{\text{PbSe}_{\{hkl\}}}) - E_{\text{ligand/PbSe}_{\{hkl\}}} \quad (1)$$

TABLE 1. Binding Energies per Ligand for $Pb(AA^-)_2$ and $Pb(OA^-)_2$ Binding to the PbSe {100} and *R* {111} Surfaces

surface	coverage of AA^- [AA^-/nm^2]	binding energy [eV/$Pb(AA^-)_2$]
	0.87	0.512
	1.3	0.523
{100}	2.6	0.577
	3.9	0.569
	5.2	0.549
	0.75	0.884
	1.5	0.887
R {111}	3.0	0.948
	4.5	0.965
	6.0	0.955

surface	coverage of OA^- [OA^-/nm^2]	binding energy [eV/$Pb(OA^-)_2$]
	1.3	0.560
{100}	2.6	0.343
	3.9	0.222
	5.2	−0.177
	1.5	0.936
R {111}	3.0	0.911
	4.5	0.559
	6.0	−0.221

where $E_{\text{ligand/PbSe}_{\{hkl\}}}$ denotes the relaxed energy of the composite system, and E_{ligand} and $E_{\text{PbSe}_{\{hkl\}}}$ refer to the relaxed energies of the isolated ligand and $\text{PbSe}_{\{hkl\}}$ slab, respectively. For the {100} surface, the Pb ion of each $Pb(AA^-)_2$ ligand was initially positioned above a surface Se ion. For the {111} surface, the Pb ion was placed in the "trench" resulting from the surface reconstruction, *i.e.*, in the position corresponding to one of the "missing" surface Pb ions. A number of geometries were attempted for the AA^- molecules in the $Pb(AA^-)_2$ ligand for a particular coverage. Here we show the binding energies for the lowest energy geometries found in each case.

Table 1 presents the calculated binding energies for the $Pb(AA^-)_2$ and $Pb(OA^-)_2$ ligands above the {100} and *R* {111} surfaces, for a range of surface coverages. We define the ligand coverage Θ as the number of carboxylate groups (*i.e.*, the number of AA^- or OA^-) per surface area. The coverage ranges from 0.87 to 5.20 OA^-/nm^2 for the {100} surface and from 0.75 to 6.00 OA^-/nm^2 for the {111} surface. The maximum coverages considered here correspond to one AA^- or OA^- species per surface unit of PbSe, which is somewhat higher than the experimentally determined ligand density for PbSe and PbS NCs, which ranges between 3.0 and 4.5 OA^-/nm[2,13,32,57] (see the Supporting Information for more information about the particular slab/ligand structures).

The $Pb(AA^-)_2$ ligands bind significantly more strongly to the *R*{111} surface than to the {100} surface. The binding energies of the $Pb(AA^-)_2$ ligands are nearly independent of coverage for both surfaces, which is similar to results from calculations for other short ligands (NH_2, PH_2, and SH) on CdSe surfaces.[58]

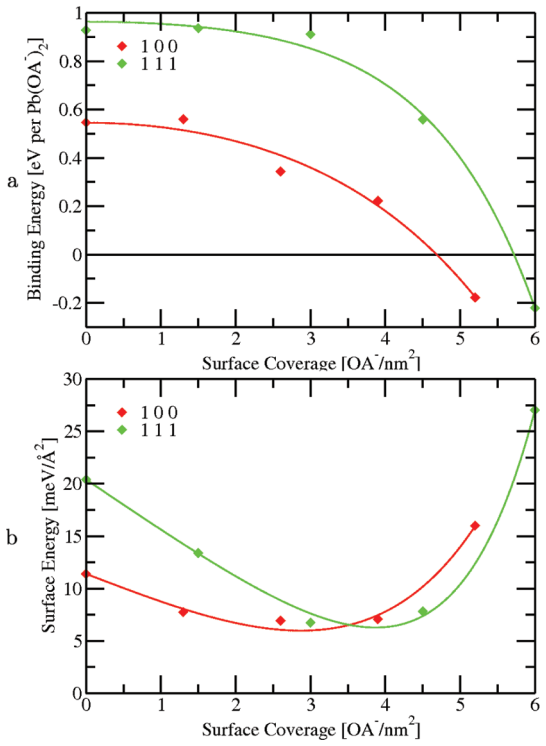

Figure 2. Binding energy (a) and surface energy (b) plotted against coverage for the PbSe {100} and *R* {111} surfaces. The binding energies were fit to a hyperbolic cosine function, as described in the main text.

For the $Pb(OA^-)_2$ ligands the binding strength decreases with increasing coverage, for both surfaces, in contrast to the $Pb(AA^-)_2$ ligands. This decrease is due to steric interactions between the long tails of the $Pb(OA^-)_2$ ligands that result in bending of the OA^- tails such that they arrange perpendicular to the surface. Near the NC edges, the steric interactions are expected to be less pronounced. This is neglected in the current study.

In the limit of low coverage, it is not too surprising that the OA^- and AA^- species exhibit similar binding energies, since the OA^- and AA^- species bind to the Pb ion through identical carboxylate groups. For the highest coverages of 5.20 OA^-/nm^2 on the {100} surface and 6.00 OA^-/nm^2 on the *R* {111} surface, the binding energy changes sign, indicating that it is energetically unfavorable for the ligands to bind to the surface at such high densities, which is consistent with the experimental measurements. To model the change in binding and surface energies with coverage, we fit a a hyperbolic cosine function (which fits the data points well) to the binding energies $E_{b,hkl}$ of the $Pb(OA^-)_2$ ligands for the surface $\{hkl\}$:

$$E_{b,\,hkl} = A + B\cosh(C\Theta_{hkl}) \qquad (2)$$

where Θ_{hkl} is the coverage on surface $\{hkl\}$ and *A*, *B*, and *C* are fitting parameters. The data and the fitted functions are shown for both surfaces in Figure 2a, and the values of the fitting parameters are given in the Supporting Information. The mean binding energy of the $Pb(AA^-)_2$ ligands was used in the fit as the binding energy at zero coverage.

For surfaces capped with ligands, the surface energy γ_{hkl} becomes a function of coverage Θ_{hkl}:

$$\gamma_{hkl} = \gamma^0_{hkl} + \Theta_{hkl}E_{b,\,hkl} \qquad (3)$$

Figure 2b shows the surface energies as a function of coverage for $Pb(OA^-)_2$ ligands on both surfaces. At low coverages, the binding energy of the ligands is approximately constant, resulting in an initial linear decrease of the surface energy γ_{hkl} with coverage. At higher coverages, the steric repulsion between the $Pb(OA)_2$ ligands leads to an increase in the surface energy. At intermediate coverages, the surface energy has a minimum corresponding to coverages of 2.9 OA^-/nm^2 for the {100} surface and 3.9 OA^-/nm^2 for the *R* {111} surface. This agrees well with experimentally determined ligand densities for Pb-salt NCs.[13,32,57]

Importantly, the variation of the {100} and {111} surface energies with ligand coverage determines the range of equilibrium core shapes available for a PbSe NC. The equilibrium shape of a crystal is given by the surface energies of the facets and is obtained through the Wulff construction

$$\frac{h_{hkl}}{h_{100}} = \frac{\gamma_{hkl}}{\gamma_{100}} \qquad (4)$$

where h_{hkl} is the distance from the center of the crystal to the $\{hkl\}$ surface, along the direction normal to the surface. Figure 3a shows the theoretically predicted equilibrium shapes that are obtained from the coverage-dependent surface energies given in eq 3. Particular values for the ratio of surface energies $\gamma_{111}/\gamma_{100}$ correspond to particular equilibrium NC shapes. For cuboctahedra $\gamma_{111}/\gamma_{100} = h_{111}/h_{100} = 2/\sqrt{3}$, for uniform (*i.e.*, Archimedean) truncated cubes $\gamma_{111}/\gamma_{100} = (1+\sqrt{2})/\sqrt{3}$, and for uniform truncated octahedra $\gamma_{111}/\gamma_{100} = \sqrt{3}/2$. For values of the ratios $\gamma_{111}/\gamma_{100} > \sqrt{3}$ and $\gamma_{111}/\gamma_{100} < 1/\sqrt{3}$ cubic and octahedral NCs, respectively, are stable. Further details relating ratios h_{111}/h_{100} to particular crystal shapes ranging between cubes and octahedra can be found in the Supporting Information. The ligand coverages on the {100} and {111} facets of a Pb-salt NC control its equilibrium shape. Changes in external conditions during or after NC synthesis can affect the ligand density and, hence, alter the NC shape; we assume an equilibrium coverage that is controlled by the concentration of the ligands in the solvent and the reaction temperature. The dependence of the equilibrium ligand coverage Θ^{equ}_{hkl} of the $\{hkl\}$ facet at ligand concentration *c* and temperature *T* follows an isotherm:

$$\Theta^{equ}_{hkl} = \frac{\frac{c}{c_0}\exp(-\Delta G/k_BT)}{1+\frac{c}{c_0}\exp(-\Delta G/k_BT)} \qquad (5)$$

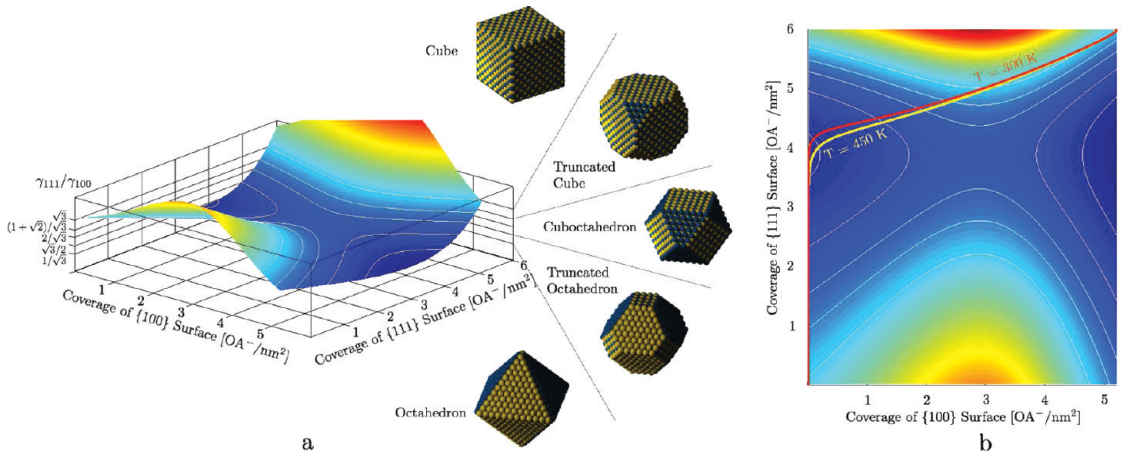

Figure 3. Surface energies and equilibrium shape of PbSe NC as a function of surface coverage. (a) Ratio of the surface energies $\gamma_{111}/\gamma_{100}$ as a function of the coverages of the {100} and {111} surfaces. The ratios $\gamma_{111}/\gamma_{100} = \sqrt{3}$, $(1 + \sqrt{2})/\sqrt{3}$, $2/\sqrt{3}$, $\sqrt{3}/2$, and $1/\sqrt{3}$ are plotted as contours on the surface and correspond to NC cores with the equilibrium shape of a cube, uniform truncated cube, cuboctahedron, uniform truncated octahedron, and octahedron, respectively. (b) Isotherms for the coverage of the {100} and {111} surfaces for temperatures $T = 300$ K (red line) and 450 K (yellow line) indicating which shapes are accessible for varying ligand concentrations. The contour lines (white) indicate the various equilibrium NC shapes as in (a).

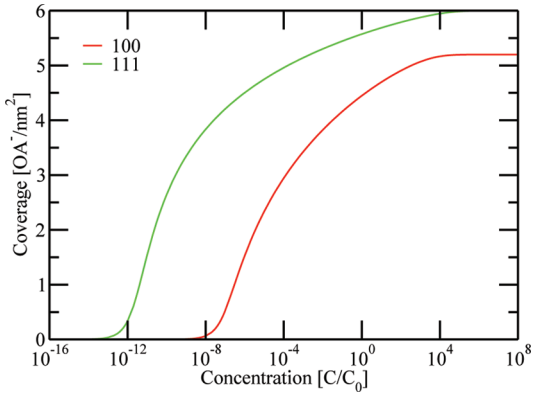

Figure 4. Isotherms for equilibrium coverage of {100} (red line) and *R* {111} (green line) surfaces at $T = 450$ K.

where k_B is Boltzmann's constant and c_0 is a reference concentration.[59] ΔG represents the free energy of interaction between the ligands and the surface, which we approximate by the binding energy $E_{b,hkl}$ of eq 2 with the fitted parameters given in the Supporting Information. In the ideal case in which $E_{b,hkl}$ is constant, eq 5 reduces to Langmuir's isotherm. For $Pb(OA^-)_2$, the binding energy $E_{b,hkl}$ given by eq 2 depends on the coverage Θ_{hkl} and the isotherm equation, eq 5, must be solved numerically to obtain Θ_{hkl}^{equ}.

We note that ΔG should also include a contribution due to the dispersion interactions between the ligands, which are not taken into account by semilocal DFT functionals, and a contribution due to interactions between the ligands and the solvent in which the NCs are dispersed, which is neglected in this work. We believe this is a reasonable approximation, since the ligand–ligand dispersion interaction at high coverages is expected to be offset by ligand–solvent dispersion interaction at low coverages for interdigitated solvent molecules. For a solvent such as hexane, both the OA^- ligand and the C_6H_{14} solvent molecule consist of hydrocarbon chains, so that interactions between them will vary similarly with separation. Molecular dynamics (MD) simulations that illustrate this point are provided in the Supporting Information.

Figure 4 shows the isotherms for the $Pb(OA^-)_2$ coverage of the {100} and *R* {111} surfaces, as a function of ligand concentration, at $T = 450$ K. The stronger binding energy of the $Pb(OA^-)_2$ to the *R* {111} surface results in a considerably higher coverage of the *R* {111} surface than of the {100} surface for all ligand concentrations. The concentration must be increased through several orders of magnitude to significantly increase the coverage on either surface. However, far lower concentrations are required in order to achieve significant coverages on the *R* {111} surface than on the {100} surface.

Figure 3b shows the coverages for the {100} and *R* {111} surfaces for $T = 300$ and 450 K that are accessible by varying the ligand concentrations in the isotherms. Importantly, the accessible coverages traverse the full range of NC core shapes, from octahedral to cubic, with increasing ligand concentration. At low concentrations only the *R* {111} surface is passivated, so that γ_{111} is much smaller than γ_{100}, leading to an octahedral equilibrium core shape. At high concentrations, on the other hand, the {100} surface is well-passivated and has a low surface energy, while excessive coverage of the *R* {111} surface increases γ_{111}, resulting in a cubic equilibrium shape. Changing the temperature from 300 to 450 K does not significantly alter the range of equilibrium NC core shapes predicted by the model.

The fact that the accessible surface coverages shown in Figure 3b traverse the range of equilibrium shapes from octahedra to cubes suggests that this entire range of shapes should be available through control

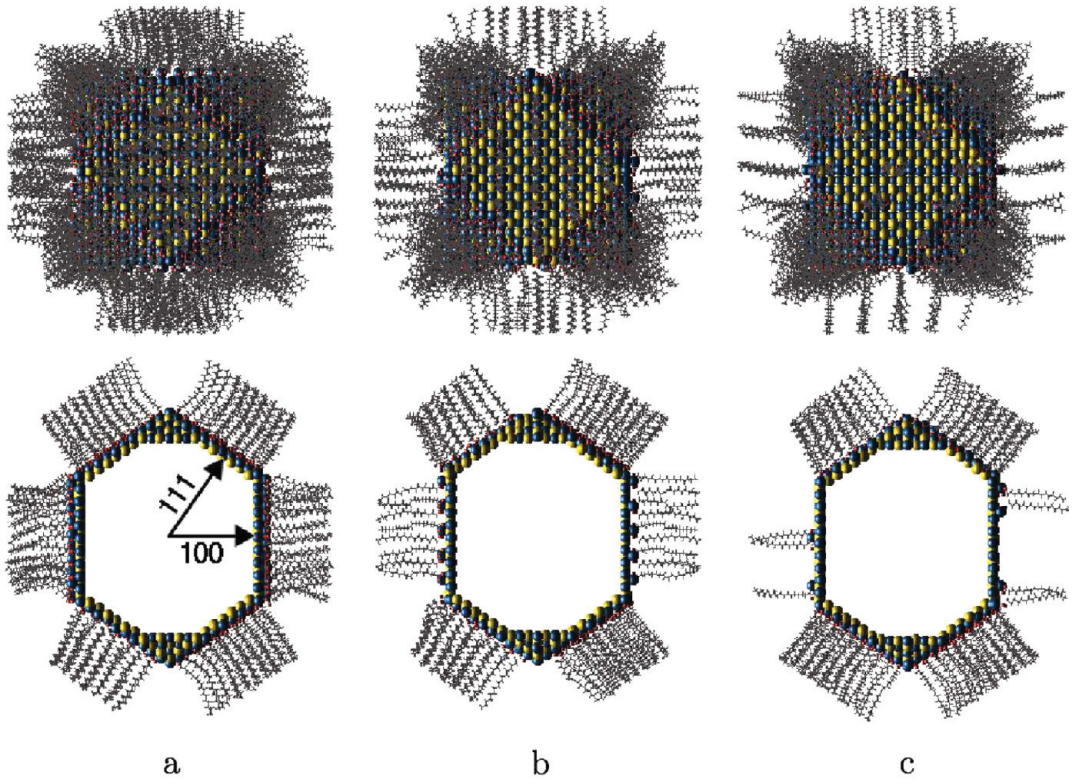

Figure 5. Oleic acid ligands (gray) are shown capping a cuboctahedral PbSe NC, illustrating the change in effective shape as the ligand coverage on the {100} facets decreases. The {100} coverage is reduced from (a) ~2.6 OA^-/nm^2, to (b) ~1.3 OA^-/nm^2, to (c) ~0.7 OA^-/nm^2. The {111} coverage is constant at ~4.5 OA^-/nm^2 for all three cases. The upper panel shows the NC viewed along the [001] direction, while the lower panel shows a central NC slice (the interior core atoms are not shown), perpendicular to the [110] direction.

of the $Pb(OA^-)_2$ ligand concentration. Our model predicts that low concentrations of $Pb(OA^-)_2$ will lead to octahedral PbSe NCs, whereas high concentrations will lead to cubic NCs. Experimental validation of this theoretical prediction is obscured by a number of factors such as time-dependent concentrations of ligands, monomers, and reaction byproduct, as well as time-dependent temperature commonly encountered in colloidal NC synthesis. The reaction temperature, reaction time, and the Pb:OA ratio are tightly coupled in the injection synthesis and are typically adjusted together in order to tune the size and shape of the resulting NCs,[47] making it difficult to delineate their separate effects. Moreels *et al*. observed that excess OA present during synthesis resulted in smaller PbSe NCs.[13] Pietryga *et al*. observed that lowering the reaction temperature decreased the size at which the NCs change from a quasi-spherical to a cubic shape.[60] Li *et al*. found that through an increase in the OA:Pb ratio it was possible to tune the NC shape from quasi-spherical, through cuboctahdral, to cubic,[53] in agreement with the predictions of our model.

In an effort to obtain further experimental support for the predicted shape control of NCs, we developed an alternative synthesis approach that encouraged the growth of particles into their equilibrium morphology. The details of this synthesis procedure are given in the Supporting Information. We performed these reactions at different OA concentrations and analyzed the products using transmission electron microscopy (TEM). While a fully systematic parameter exploration is beyond the scope of this work, a greater amount of {100} faceting in the particles synthesized with a higher OA concentration suggests that these NCs have a more cubic-like shape. TEM micrographs showing samples grown at OA:Pb ratios of 1:4, 1:1, 2:1, and 10:1 are given in Figure 6, along with the normalized integrated ratio of the intensities of the {111} and {200} peaks obtained from X-ray diffraction (XRD) of the drop-cast PbSe NC films, for each concentration. The increased {100} faceting is consistent with a transition to a more cubic shape of NC as the ratio is increased. For the NCs synthesized at the OA:Pb ratio of 1:4, the NCs appear to have assembled into chain-like aggregates, while the assemblies are more isotropic when more OA was included in the reaction. It is possible that a transition toward octahedral-shaped particles for lower OA:Pb ratios is related to the increased tendency of these NCs to form linear aggregates.

The composition of PbSe NCs has been previously determined using inductively coupled plasma mass spectrometry (ICP-MS); a Pb:Se ratio of approximately 1.24−1.36:1 was observed for 5.7 nm NCs.[50] Our model predicts that one excess Pb^{2+} cation will be present for

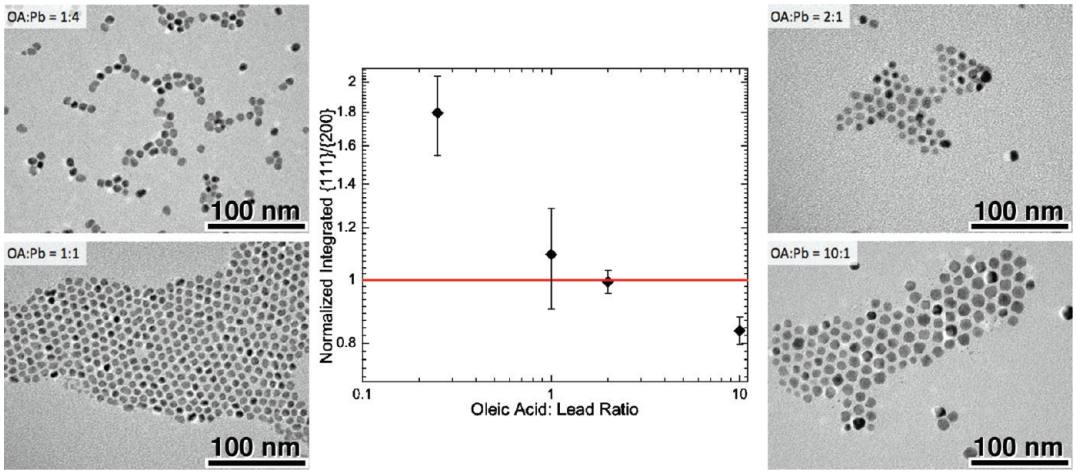

Figure 6. Normalized ratio of the integrated intensity peaks corresponding to {111} and {200} planes obtained using XRD for films of PbSe NCs, synthesized at different OA:Pb ratios. The decrease in the {111}/{200} ratio indicates a clear trend toward larger {100} faceting for NCs produced at higher OA:Pb ratios.

every two OA^- anions, which does not agree with a report from the literature, in which a ratio of 1:1 was observed.[13] Furthermore, considering a 5.7 nm NC within our model, the ratio of Pb:Se is expected to be somewhat lower than the values obtained using ICP-MS, varying between 1.09 and 1.17:1 (see Supporting Information for further details of this calculation). Stoichiometries close to those determined by ICP-MS are obtained if all NC surfaces site are terminated by Pb. We speculate that this observed *additional* excess Pb may be due to the presence of neutral Pb^0 atoms physisorbed at the surface or Pb^{2+} cations bound to some alternative counterion. For example, $Pb(Cl^-)_2$ was observed to be present at the surface of PbS NCs synthesized using $PbCl_2$ and elemental sulfur.[57] In the case that Cl^- is not present in the reaction, other possible candidate counterions are OH^- and O^{2-}. X-ray photoelectron spectroscopy (XPS) studies have found neither $Pb(OH^-)_2$ or PbO^{2-} to be present in any appreciable amounts for freshly synthesized PbSe NCs, however.[38] Binding energies calculated using DFT for PbO^{2-} and $Pb(OH^-)_2$ on the {100} surface show only weak binding ($\lesssim$ 0.4 eV per PbO^{2-} or $Pb(OH^-)_2$), consistent with these measurements. Furthermore, significant numbers of OH^- groups are unlikely to be present in the solution, since the synthesis reactions we have carried out take place under mildly acidic conditions. Given the weak binding of the PbO^{2-} and $Pb(OH^-)_2$ and their likely scarcity, as well as the XPS results, we tentatively ascribe the deficit of excess Pb predicted by our model to Pb^0, but suggest that this remains an important area for further study. In any case, the additional excess Pb is not expected to be attached to ligands with long, bulky chains, and since short ligands interact with each other laterally very little (as shown by the $Pb(AA^-)_2$ adsorption energy results given in Table 1 or the binding energy calculations reported by Csik *et al.*[58]), the maximum possible amount of $Pb(OA^-)_2$ at the surface need not be limited as a result of their presence. Absent further information about the nature of the additional excess Pb, we consider the simplifying assumption that all surfaces sites not passivated by $Pb(OA^-)_2$ are instead uniformly capped by some Pb-containing group, such as Pb^0 or $Pb^{2+}X^{2-}$, where X is a short ligand. In this case the {100} and {111} surface energy curves shown in Figure 2 each could be shifted by a constant amount. Such a shift would alter the particular values of the ratio $\gamma_{111}/\gamma_{100}$ for each concentration along the isotherm, but would not alter the general trend predicted by the isotherms of Figure 3, that higher OA concentrations should lead to increased {100} faceting. We also note that the neglect of the NC edges in our model may contribute slightly to the predicted Pb:Se ratio being lower than that observed in the experiments.

The isotherms shown in Figure 4 and the accessible coverages of the {100} and {111} surfaces shown in Figure 3b suggest that varying the ligand concentrations significantly changes the relative coverage of the two facets. When NCs are aged at ambient temperature in an environment with reduced ligand concentration,[32] the shape of the inorganic NC core is not expected to change significantly. However, the different detachment of ligands from the {100} and {111} facets will change the effective shape of the NC/ligand system. The ligand coverage of the {100} facets decreases more quickly with reduced ligand concentration than that of the {111} facets. Figure 5 illustrates the change in effective shape for NCs for which the ligand coverage decrease follows the curve in Figure 3b. The structures shown are taken from low-temperature MD simulations at each coverage, carried out using the LAMMPS package[61] and the Reax force field[62] for the ligands. Although MD simulations employing empirical potentials such as the Reax force field could be useful for describing the strength of the

dispersion forces between ligands, a complete model must also account for the interactions between the ligands and the surrounding solvent, which are expected to largely offset the change in ligand–ligand dispersion interactions with coverage (see Supporting Information). The MD simulations described here, which do not describe the solvent, are used only to illustrate the effect of ligand coverage on the effective NC shape. The rapid decrease in the coverage of the {100} facets with reduced ligand concentration results in a strongly anisotropic effective shape of the NC/ligand system. This is consistent with the preference for *bcc* packing in aged PbSe NC superlattices[32] and suggests that the effective shape of the NCs in the assembly is particularly sensitive to the coverage of the {100} facets.

CONCLUSIONS

Through consideration of the surface–ligand interactions in the PbSe NC system, we have constructed a model that predicts that the facet-dependent interactions between core and ligand capping layer can be exploited, through the ligand concentration, to allow control over the morphology both of individual NCs and of their assembly. Density functional calculations determined surface and binding energies for PbSe {100} and reconstructed {111} surfaces, capped with $Pb(OA^-)_2$ for a range of coverages relevant to experiments. The change in surface energies with ligand coverage of these two surfaces is predicted to give rise to equilibrium NC shapes ranging from octahedra to cuboctahedra to cubes, in accordance with experimentally observed shapes of Pb-salt NCs capped with OA^-. Preliminary experiments using an *ad hoc* synthesis procedure support the general trend predicted by our model, as do other reports from the literature.[53] Further experiments are required to assess whether the ligand concentration is a viable method of shape control for the Pb-salt NCs. We predict a more rapid decrease in the ligand coverage of the {100} facets than the {111} facets with reduced ligand concentration. This results in a strongly anisotropic effective shape of the NC/ligand system and helps explain experimentally observed changes in the symmetry of NC assembly. The ability to tune the morphology of individual NCs and their assembly would present significant advantages for the design of NC-based materials for applications. Since facet-specific ligand data and adsorption and surface energies are not easily accessible by experiments, computer modeling and simulation provide a useful approach to predict and assess the differences in surface chemistry between facets and the resulting NC core shape and effective shape of the NC–ligand system. We expect that the possibility to control NC morphology through facet-specific surfactant interactions will remain an important area for further study.

METHODS

Computational Approach. Surface energy and ligand binding energy DFT calculations were carried out using the Vienna Ab initio Simulation Package (VASP)[63–66] with a plane wave basis set and periodic boundary conditions. The projector augmented wave method was used to describe the interactions between ions and electrons, and the tetrahedron method with Blöchl corrections[67] was used to perform the Brillouin zone integration. Special k-points were generated using the Monkhorst–Pack method, with k-point meshes chosen such that the k-point density along the reciprocal lattice vectors is about 60 per $Å^{-1}$. The generalized gradient PBE exchange–correlation functional[68] was used. The cutoff energy for the wave functions was varied between 211 and 360 eV for calculations of the PbSe bare surface energies and was increased to 400 eV for calculations of the ligand binding energies, owing to the harder pseudopotentials of the C and O atoms in the ligand.

Conflict of Interest: The authors declare no competing financial interest.

Acknowledgment. This work was supported in part by Award No. KUS-C1-018-02, made by King Abdullah University of Science and Technology (KAUST). This research used computational resources of the Computation Center for Nanotechnology Innovation at Rensselaer Polytechnic Institute and was supported in part by the National Science Foundation through TeraGrid computational resources provided by the National Center for Supercomputing Applications, the Texas Advanced Computing Center, and the Louisiana Optical Network Initiative under Grant No. DMR050036

Supporting Information Available: Experimental information; evaluation of calculated ligand geometries; further details of computational approach; molecular dynamics simulations of ligand–ligand and ligand–solvent interactions; parameter fit for the binding energies; Pb:Se ratio predicted by the model; ratios h_{111}/h_{100} for particular NC shapes. This material is available free of charge *via* the Internet at http://pubs.acs.org.

REFERENCES AND NOTES

1. Nirmal, M.; Norris, D. J.; Kuno, M.; Bawendi, M. G.; Efros, A. L.; Rosen, M. Observation of the "Dark Exciton" in CdSe Quantum Dots. *Phys. Rev. Lett.* **1995**, *75*, 3728–3731.
2. Alivisatos, A. P. Semiconductor Clusters, Nanocrystals, and Quantum Dots. *Science* **1996**, *271*, 933–937.
3. El-Sayed, M. A. Small Is Different: Shape-, Size-, and Composition-Dependent Properties of Some Colloidal SemiconductorNanocrystals. *Acc. Chem. Res.* **2004**, *37*, 326–333.
4. Murray, C. B.; Norris, D. J.; Bawendi, M. G. Synthesis and Characterization of Nearly Monodisperse CdE (E = Sulfur, Selenium, Tellurium) Semiconductor Nanocrystallites. *J. Am. Chem. Soc.* **1993**, *115*, 8706–8715.
5. Peng, X.; Manna, L.; Yang, W.; Wickham, J.; Scher, E.; Kadavanich, A.; Alivisatos, A. P. Shape Control of CdSe Nanocrystals. *Nature* **2000**, *404*, 59–61.
6. Korgel, B. A.; Fitzmaurice, D. Self-Assembly of Silver Nanocrystals into Two-Dimensional Nanowire Arrays. *Adv. Mater.* **1998**, *10*, 661–665.

7. Puntes, V. F.; Zanchet, D.; Erdonmez, C. K.; Alivisatos, A. P. Synthesis of hcp-Co Nanodisks. *J. Am. Chem. Soc.* **2002**, *124*, 12874–12880.
8. Manna, L.; Scher, E. C.; Alivisatos, A. P. Synthesis of Soluble and Processable Rod-, Arrow-, Teardrop-, and Tetrapod-Shaped CdSe Nanocrystals. *J. Am. Chem. Soc.* **2000**, *122*, 12700–12706.
9. Cho, K.; Talapin, D. V.; Gaschler, W.; Murray, C. B. Designing PbSe Nanowires and Nanorings through Oriented Attachment of Nanoparticles. *J. Am. Chem. Soc.* **2005**, *127*, 7140–7147.
10. Yin, Y.; Alivisatos, A. P. Colloidal Nanocrystal Synthesis and the Organic-Inorganic Interface. *Nature* **2005**, *437*, 664–670.
11. Penn, R. L.; Banfield, J. F. Morphology Development and Crystal Growth in Nanocrystalline Aggregates under Hydrothermal Conditions: Insights from Titania. *Geochim. Cosmochim. Acta* **1999**, *63*, 1549–1557.
12. Pradhan, N.; Reifsnyder, D.; Xie, R.; Aldana, J.; Peng, X. Surface Ligand Dynamics in Growth of Nanocrystals. *J. Am. Chem. Soc.* **2007**, *129*, 9500–9509.
13. Moreels, I.; Fritzinger, B.; Martins, J. C.; Hens, Z. Surface Chemistry of Colloidal PbSe Nanocrystals. *J. Am. Chem. Soc.* **2008**, *130*, 15081–15086.
14. Kilina, S.; Ivanov, S.; Tretiak, S. Effect of Surface Ligands on Optical and Electronic Spectra of Semiconductor Nanoclusters. *J. Am. Chem. Soc.* **2009**, *131*, 7717–7726.
15. Fritzinger, B.; Capek, R. K.; Lambert, K.; Martins, J. C.; Hens, Z. Utilizing Self-Exchange To Address the Binding of Carboxylic Acid Ligands to CdSe Quantum Dots. *J. Am. Chem. Soc.* **2010**, *132*, 10195–10201.
16. Bian, K.; Choi, J. J.; Kaushik, A.; Clancy, P.; Smilgies, D.; Hanrath, T. Shape-Anisotropy Driven Symmetry Transformations in Nanocrystal Superlattice Polymorphs. *ACS Nano* **2011**, *5*, 2815–2823.
17. Yu, D.; Wang, C.; Guyot-Sionnest, P. n-Type Conducting CdSe Nanocrystal Solids. *Science* **2003**, *300*, 1277–1280.
18. Talapin, D. V.; Murray, C. B. PbSe Nanocrystal Solids for n- and p-Channel Thin Film Field-Effect Transistors. *Science* **2005**, *310*, 86–89.
19. Law, M.; Luther, J. M.; Song, Q.; Hughes, B. K.; Perkins, C. L.; Nozik, A. J. Structural, Optical, and Electrical Properties of PbSe Nanocrystal Solids Treated Thermally or with Simple Amines. *J. Am. Chem. Soc.* **2008**, *130*, 5974–5985.
20. Liu, Y.; Gibbs, M.; Puthussery, J.; Gaik, S.; Ihly, R.; Hillhouse, H. W.; Law, M. Dependence of Carrier Mobility on Nanocrystal Size and Ligand Length in PbSe Nanocrystal Solids. *Nano Lett.* **2010**, *10*, 1960–1969.
21. Nag, A.; Kovalenko, M. V.; Lee, J.; Liu, W.; Spokoyny, B.; Talapin, D. V. Metal-Free Inorganic Ligands for Colloidal-Nanocrystals: S^{2-}, HS^{-}, Se^{2-}, HSe^{-}, Te^{2-}, HTe^{-}, $TeS3^{2-}$, OH^{-}, and NH^{2-} as Surface Ligands. *J. Am. Chem. Soc.* **2011**, *133*, 10612–10620.
22. Lidke, D. S.; Nagy, P.; Heintzmann, R.; Arndt- Jovin, D. J.; Post, J. N.; Grecco, H. E.; Jares-Erijman, E. A.; Jovin, T. M. Quantum Dot Ligands Provide New Insights into erbB/HER Receptor-Mediated Signal Transductioneceptor-Mediated Signal Transduction. *Nat. Biotechnol.* **2004**, *22*, 198–203.
23. Mason, J.; Farmer, H.; Tomlinson, I.; Schwartz, J.; Savchenko, V.; DeFelice, L.; Rosenthal, S.; Blakely, R. Novel Fluorescence-based Approaches for the Study of Biogenic Amine Transporter Localization, Activity, and Regulationctivity, and Regulation. *J. Neurosci. Methods* **2005**, *143*, 3–25.
24. Vu, T. Q.; Maddipati, R.; Blute, T. A.; Nehilla, B. J.; Nusblat, L.; Desai, T. A. Peptide-Conjugated Quantum Dots Activate Neuronal Receptors and Initiate Downstream Signaling of Neurite Growth. *Nano Lett.* **2005**, *5*, 603–607.
25. Fu, A.; Gu, W.; Larabell, C.; Alivisatos, A. P. Semiconductor Nanocrystals for Biological Imaging. *Curr. Opin. Neurobiol.* **2005**, *15*, 568–575. PMID: 16150591.
26. Pradhan, N.; Battaglia, D. M.; Liu, Y.; Peng, X. Efficient, Stable, Small, and Water-Soluble Doped ZnSe Nanocrystal Emitters as Non-Cadmium Biomedical Labels. *Nano Lett.* **2007**, *7*, 312–317.
27. Kuno, M.; Lee, J. K.; Dabbousi, B. O.; Mikulec, F. V.; Bawendi, M. G. The Band Edge Luminescence of Surface Modified CdSe Nanocrystallites: Probing the Luminescing State. *J. Chem. Phys.* **1997**, *106*, 9869–9882.
28. Bakueva, L.; Musikhin, S.; Hines, M. A.; Chang, T. F.; Tzolov, M.; Scholes, G. D.; Sargent, E. H. Size-Tunable Infrared (1000−1600 nm) Electroluminescence from PbS Quantum-Dot Nanocrystals in a Semiconducting Polymer. *Appl. Phys. Lett.* **2003**, *82*, 2895–2897.
29. Beard, M. C.; Midgett, A. G.; Law, M.; Semonin, O. E.; Ellingson, R. J.; Nozik, A. J. Variations in the Quantum Efficiency of Multiple Exciton Generation for a Series of Chemically Treated PbSe Nanocrystal Films. *Nano Lett.* **2009**, *9*, 836–845.
30. Shevchenko, E.; Talapin, D.; Kornowski, A.; Wiekhorst, F.; Kötzler, J.; Haase, M.; Rogach, A.; Weller, H. Colloidal Crystals of Monodisperse FePt Nanoparticles Grown by a Three-Layer Technique of Controlled Oversaturation. *Adv. Mater.* **2002**, *14*, 287–290.
31. Urban, J. J.; Talapin, D. V.; Shevchenko, E. V.; Murray, C. B. Self-Assembly of PbTe Quantum Dots into Nanocrystal Superlattices and Glassy Films. *J. Am. Chem. Soc.* **2006**, *128*, 3248–3255.
32. Choi, J. J.; Bealing, C. R.; Bian, K.; Hughes, K. J.; Zhang, W.; Smilgies, D.; Hennig, R. G.; Engstrom, J. R.; Hanrath, T. Controlling Nanocrystal Superlattice Symmetry and Shape-Anisotropic Interactions through Variable Ligand Surface Coverage. *J. Am. Chem. Soc.* **2011**, *133*, 3131–3138.
33. Burda, C.; Chen, X.; Narayanan, R.; El-Sayed, M. A. Chemistry and Properties of Nanocrystals of Different Shapes. *Chem. Rev.* **2005**, *105*, 1025–1102.
34. Herring, C. Some Theorems on the Free Energies of Crystal Surfaces. *Phys. Rev.* **1951**, *82*, 87–93.
35. Polarz, S. Shape Matters: Anisotropy of the Morphology of Inorganic Colloidal Particles−Synthesis and Function. *Adv. Func. Mater.* **2011**, *21*, 3214–3230.
36. Chiu, C.-Y.; Li, Y.; Ruan, L.; Ye, X.; Murray, C. B.; Huang, Y. Platinum Nanocrystals Selectively Shaped Using Facet-Specific Peptide Sequences. *Nat. Chem.* **2011**, *3*, 393–399.
37. Wise, F. W. Lead Salt Quantum Dots: the Limit of Strong Quantum Confinement. *Acc. Chem. Res.* **2000**, *33*, 773–780.
38. Luther, J. M.; Law, M.; Beard, M. C.; Song, Q.; Reese, M. O.; Ellingson, R. J.; Nozik, A. J. Schottky Solar Cells Based on Colloidal Nanocrystal Films. *Nano Lett.* **2008**, *8*, 3488–3492.
39. Ma, W.; Luther, J. M.; Zheng, H.; Wu, Y.; Alivisatos, A. P. Photovoltaic Devices Employing Ternary PbS_xSe_{1-x} Nanocrystals. *Nano Lett.* **2009**, *9*, 1699–1703.
40. Choi, J. J.; Lim, Y.-F.; Santiago-Berrios, M. B.; Oh, M.; Hyun, B.-R.; Sun, L.; Bartnik, A. C.; Goedhart, A.; Malliaras, G. G.; Abruña, H. D.; *et al*. PbSe Nanocrystal Excitonic Solar Cells. *Nano Lett.* **2009**, *9*, 3749–3755.
41. McDonald, S. A.; Konstantatos, G.; Zhang, S.; Cyr, P. W.; Klem, E. J. D.; Levina, L.; Sargent, E. H. Solution-Processed PbS Quantum Dot Infrared Photodetectors and Photovoltaics. *Nat. Mater.* **2005**, *4*, 138–142.
42. Jiang, X.; Schaller, R. D.; Lee, S. B.; Pietryga, J. M.; Klimov, V. I.; Zakhidov, A. A. PbSe Nanocrystal/Conducting Polymer Solar Cells with an Infrared Response to 2 Micron. *J. Mater. Res.* **2007**, *22*, 2205–2210.
43. Zhao, N.; Osedach, T. P.; Chang, L.; Geyer, S. M.; Wanger, D.; Binda, M. T.; Arango, A. C.; Bawendi, M. G.; Bulovic, V. Colloidal PbS Quantum Dot Solar Cells with High Fill Factor. *ACS Nano* **2010**, *4*, 3743–3752.
44. Pattantyus-Abraham, A. G.; Kramer, I. J.; Barkhouse, A. R.; Wang, X.; Konstantatos, G.; Debnath, R.; Levina, L.; Raabe, I.; Nazeeruddin, M. K.; Grätzel, M.; *et al*. Depleted-Heterojunction Colloidal Quantum Dot Solar Cells. *ACS Nano* **2010**, *4*, 3374–3380.
45. Vercelli, B.; Zotti, G.; Berlin, A.; Natali, M. Self- Assembled Structures of Semiconductor Nanocrystals and Polymers for Photovoltaics. (3) PbSe Nanocrystal-Polymer LBL Multilayers. Optical, Electrochemical, Photoelectrochemical, and Photoconductive Properties. *Chem. Mater.* **2010**, *22*, 2001–2009.

46. Argeri, M.; Fraccarollo, A.; Grassi, F.; Marchese, L.; Cossi, M. Density Functional TheoryModeling of PbSe Nanoclusters: Effect of Surface Passivation on Shape and Composition. *J. Phys. Chem. C* **2011**, *115*, 11382–11389.
47. Hanrath, T.; Veldman, D.; Choi, J. J.; Christova, C. G.; Wienk, M. M.; Janssen, R. A. J. PbSe Nanocrystal Network Formation during Pyridine Ligand Displacement. *ACS Appl. Mater. Interfaces* **2009**, *1*, 244–250.
48. Fang, C.; van Huis, M. A.; Vanmaekelbergh, D.; Zandbergen, H. W. Energetics of Polar and Nonpolar Facets of PbSe Nanocrystals from Theory and Experiment. *ACS Nano* **2010**, *4*, 211–218.
49. Shevchenko, E. V.; Talapin, D. V.; Kotov, N. A.; O'Brien, S.; Murray, C. B. Structural Diversity in Binary Nanoparticle Superlattices. *Nature* **2006**, *439*, 55–59.
50. Moreels, I.; Lambert, K.; Muynck, D. D.; Vanhaecke, F.; Poelman, D.; Martins, J. C.; Allan, G.; Hens, Z. Composition and Size-Dependent Extinction Coefficient of Colloidal PbSe Quantum Dots. *Chem. Mater.* **2007**, *19*, 6101–6106.
51. Petkov, V.; Moreels, I.; Hens, Z.; Ren, Y. PbSe Quantum Dots: Finite, Off-Stoichiometric, and Structurally Distorted. *Phys. Rev. B* **2010**, *81*, 241304.
52. Dai, Q.; Wang, Y.; Li, X.; Zhang, Y.; Pellegrino, D. J.; Zhao, M.; Zou, B.; Seo, J.; Wang, Y.; Yu, W. W. Size- Dependent Composition and Molar Extinction Coefficient of PbSe Semiconductor Nanocrystals. *ACS Nano* **2009**, *3*, 1518–1524.
53. Li, H.; Chen, D.; Li, L.; Tang, F.; Zhang, L.; Ren, J. Size- and Shape-Controlled Synthesis of PbSe and PbS Nanocrystals via a Facile Method. *Cryst. Eng. Chem.* **2010**, *12*, 1127–1133.
54. Kimura, K.; Nakajima, K.; Fujii, Y.; Mannami, M. Observation of the PbSe(111) Surface using High- Resolution Rutherford Backscattering Spectroscopy. *Surf. Sci.* **1994**, *318*, 363–367.
55. Barbier, A.; Mocuta, C.; Kuhlenbeck, H.; Peters, K. F.; Richter, B.; Renaud, G. Atomic Structure of the Polar NiO(111)-p (2 × 2) Surface. *Phys. Rev. Lett.* **2000**, *84*, 2897–2900.
56. Kutana, A.; Erwin, S. C. PbSe Nanocrystals Remain Intrinsic after Surface Adsorption of Hydrazine. *Phys. Rev. B* **2011**, *83*, 235419.
57. Moreels, I.; Justo, Y.; De Geyter, B.; Haustraete, K.; Martins, J. C.; Hens, Z. Size-Tunable, Bright, and Stable PbS Quantum Dots: A Surface Chemistry Study. *ACS Nano* **2011**, *5*, 2004–2012.
58. Csik, I.; Russo, S. P.; Mulvaney, P. Density Functional Study of Surface Passivation of Nonpolar Wurtzite CdSe Surfaces. *J. Phys. Chem. C* **2008**, *112*, 20413–20417.
59. Tsao, J. Y. *Materials Fundamentals of Molecular Beam Epitaxy*; Academic Press: New York, 1992.
60. Pietryga, J. M.; Schaller, R. D.; Werder, D.; Stewart, M. H.; Klimov, V. I.; Hollingsworth, J. A. Pushing the Band Gap Envelope:Mid-Infrared Emitting Colloidal PbSe Quantum Dots. *J. Am. Chem. Soc.* **2004**, *126*, 11752–11753.
61. Plimpton, S. Fast Parallel Algorithms for Short-Range Molecular Dynamics. *J. Comput. Phys.* **1995**, *117*, 1–19.
62. Chenoweth, K.; van Duin, A. C. T.; Goddard, W. A. ReaxFF Reactive Force Field for Molecular Dynamics Simulations of Hydrocarbon Oxidation. *J. Phys. Chem. A* **2008**, *112*, 1040–1053.
63. Kresse, G.; Hafner, J. Ab InitioMolecular Dynamics for Liquid Metals. *Phys. Rev. B* **1993**, *47*, 558–561.
64. Kresse, G.; Hafner, J. Ab Initio Molecular-Dynamics Simulation of the Liquid-Metal-Amorphous-Semiconductor Transition in Germanium. *Phys. Rev. B* **1994**, *49*, 14251–14269.
65. Kresse, G.; Furthmüller, J. Efficiency of Ab-Initio Total Energy Calculations for Metals and Semiconductors using a Plane-Wave Basis Set. *Comput. Mater. Sci.* **1996**, *6*, 15–50.
66. Kresse, G.; Furthmüller, J. Efficient Iterative Schemes for Ab Initio Total-Energy Calculations using a Plane-Wave Basis Set. *Phys. Rev. B* **1996**, *54*, 11169–11186.
67. Blöchl, P. E.; Jepsen, O.; Andersen, O. K. Improved Tetrahedron Method for Brillouin-Zone Integrations. *Phys. Rev. B* **1994**, *49*, 16223–16233.
68. Perdew, J. P.; Burke, K.; Ernzerhof, M. Generalized Gradient Approximation Made Simple. *Phys. Rev. Lett.* **1996**, *77*, 3865–3868.